The Astrophysical Journal, 585:617–629, 2003 March 10

PREDICTIONS FOR COSMOLOGICAL INFRARED SURVEYS FROM SPACE WITH THE MULTIBAND IMAGING PHOTOMETER FOR *SIRTF*

H. Dole
Steward Observatory, University of Arizona, 933 North Cherry Avenue, Tucson, AZ 85721; hdole@as.arizona.edu

and

G. Lagache and J.-L. Puget
Institut d'Astrophysique Spatiale, bât 121, Université Paris Sud, F-91405 Orsay CEDEX, France
Received 2002 August 15; accepted 2002 November 14

ABSTRACT

We make predictions for the cosmological surveys to be conducted by the Multiband Imaging Photometer for *SIRTF* (MIPS) at 24, 70, and 160 μm for the Guaranteed Time Observer and the Legacy programs, using the latest knowledge of the instrument. In addition to the detector noise and the cirrus confusion noise, we discuss in detail the derivation of the confusion noise due to extragalactic sources, which depends strongly on the shape of the source counts at a given wavelength and on the telescope and detector pixel sizes. We show that it is wise in general to compare the classical photometric criterion, used for decades, and the so-called source density criterion to predict the confusion levels. We obtain, using the model of Lagache, Dole, and Puget, limiting fluxes of 50 μJy, 3.2 mJy, and 36 mJy at 24, 70, and 160 μm, respectively. After taking into account other known sources of noise that will limit the surveys' sensitivities, we compute the redshift distributions of the detected sources at each wavelength and show that they extend up to $z \sim 2.7$ at 24 μm and up to $z \sim 2.5$ at 70 and 160 μm, leading to the resolution of at most 69%, 54%, and 24% of the cosmic infrared background (CIB) at 24, 70, and 160 μm, respectively. We estimate which galaxy populations will be used to derive the luminosity function evolution with redshift. We also give the redshift distributions of the unresolved sources in the far-IR range, which dominates the fluctuations of the CIB, and a predicted power spectrum showing the feasibility of fluctuations (due to both Poissonian and clustered source distributions) measurements. The main conclusion is that MIPS (and *SIRTF* in general) cosmological surveys will greatly improve our understanding of galaxy evolution by giving data with unprecedented accuracy in the mid-IR and far-IR range.

Subject headings: cosmology: observations — infrared: galaxies — galaxies: evolution — methods: observational

1. INTRODUCTION

The *Infrared Space Observatory* (*ISO*) performed deep surveys in the mid-IR (MIR) and far-IR (FIR) range (see Genzel & Cesarsky 2000; Franceschini et al. 2001 for reviews) in order to study galaxy evolution and to constrain the global star formation rate. Together with other surveys performed from the ground (e.g., with SCUBA and MAMBO), our view of galaxy evolution in the infrared, submillimeter, and millimeter range became more accurate.

With the information extracted from these cosmological surveys, and in particular from the source counts, the redshift distribution of the sources, the spectral energy distribution (SED) of the cosmic infrared background (CIB), and the analysis of the CIB fluctuations, it is possible to build a coherent view of galaxy evolution and formation in the infrared and submillimeter range by developing models that fit all the available data. Many semiempirical models exist (Roche & Eales 1999; Tan, Silk, & Balland 1999; Devriendt & Guiderdoni 2000; Dole et al. 2000; Wang & Biermann 2000; Chary & Elbaz 2001; Franceschini et al. 2001; Malkan & Stecker 2001; Pearson 2001; Rowan-Robinson 2001a, 2001b; Takeuchi et al. 2001; Xu et al. 2001; Wang 2002) and try to address questions about the evolution of infrared galaxies, inferring the global star formation rate. These models fit the data reasonably well. Recently, Lagache, Dole, & Puget (2003) have developed a phenomenological model that satisfies all the present observational constraints, one of which is the fluctuations of the background, as a powerful tool for investigating future observations.

The availability of new space facilities in the coming years, such as the *Space Infrared Telescope Facility* (*SIRTF*) in early 2003, *ASTRO-F*, and later in the decade, *Planck* and *Herschel*, and on the ground the Atacama Large Millimeter Array (ALMA), opens new perspectives to study in detail the population of infrared galaxies beyond $z = 1$. Which galaxy populations will these facilities be able to detect? What fraction of the CIB will be resolved into sources? Up to what redshift will it be possible to construct a luminosity function and detect any evolution? What will be the observational limitations on the cosmological surveys?

To answer most of these questions prior to any new data being taken and to better plan the surveys that will fully use the capabilities of these new facilities, it is common to use models to make predictions according to today's knowledge. The goal of this paper is to investigate the properties (e.g., confusion, sensitivity, redshift distributions) of the planned *SIRTF* surveys with the Multiband Imaging Photometer for *SIRTF* (MIPS), using the Lagache et al. (2003) model as well as the latest knowledge of the MIPS instrument. Detailed predictions for *Herschel*, *Planck*, and ALMA are given in Lagache et al. (2003).

The structure of the paper is as follows: The MIPS instrument and the planned surveys are described in § 2. We discuss the confusion noise due to Galactic cirrus in § 3. In § 4 we summarize the Lagache et al. (2003) model and in § 5

one of its applications: the generation of multiwavelength maps. The general case of the confusion noise due to extragalactic sources is discussed in § 6, and the confusion limits for MIPS are given in § 7. The total sensitivity for the surveys is given in § 8. We discuss the expected results regarding resolved sources in § 9 and regarding the unresolved sources in § 10.

2. THE MIPS INSTRUMENT AND THE PLANNED COSMOLOGICAL SURVEYS

2.1. *MIPS*

MIPS[1] (Rieke et al. 1984; Young et al. 1998; Heim et al. 1998) is one of the three *SIRTF* (Werner & Fanson 1995) focal plane instruments, the others being the Infrared Array Camera (IRAC; Fazio et al. 1998) and the Infrared Spectrograph (IRS; Houck & Van Cleve 1995). MIPS is composed of three large-array detectors, sensitive at 24, 70, and 160 μm, respectively. The array sizes are 128^2, 32^2, and 2×20 pixels, and the detector material is Si:As BIB, Ge:Ga, and stressed Ge:Ga, respectively. Among the main key features of MIPS are (1) the large size of the arrays, (2) the technical achievements in the detectors, (3) the calibration strategy of the FIR arrays (Engelbracht et al. 2000), with frequent stimulator flashes tracking the responsivity variations, and (4) the presence of a scan mirror allowing an efficient and redundant sky coverage of 5′-wide stripes, simultaneously at all three wavelengths.

The beam profile characteristics play an important role in computing the confusion limits; they have been generated using the S Tiny Tim software, which is an updated version for *SIRTF* of the Tiny Tim software for the *Hubble Space Telescope* (Krist 1993). Table 1 summarizes the main characteristics of the pixels and beam profiles for MIPS.

TABLE 1

SOME MIPS INSTRUMENTAL CHARACTERISTICS: PIXEL SIZE, BEAM PROFILE, AND NOISE

Characteristic	24 μm	70 μm	160 μm
Pixel size (arcsec)	2.55	9.84	16.0
FWHM[a] (arcsec)	5.6	16.7	35.2
Pixel solid angle (sr)	1.41×10^{-10}	2.30×10^{-9}	5.87×10^{-9}
$\int f(\theta,\phi)d\theta\, d\phi$[b] (sr)	1.25×10^{-9}	9.98×10^{-9}	4.45×10^{-8}
$\int f^2(\theta,\phi)d\theta\, d\phi$[c] (sr)	4.27×10^{-10}	3.45×10^{-9}	1.66×10^{-8}
1 σ_p for 10 s integration[d] (mJy)	0.22	2.0	6.6

[a] Measured from S Tiny Tim models.
[b] Integral of the beam profile $f(\theta,\phi)$.
[c] Integral of the squared beam profile $f^2(\theta,\phi)$ (used in eq. [5]).
[d] The 1 σ photon (and instrumental) noise for a 10 s integration, for both scan map and photometry modes (G. H. Rieke 2002, private communication).

2.2. *Cosmological Surveys with MIPS*

The currently planned cosmological surveys with MIPS are mainly scheduled through two types of programs: the Guaranteed Time Observer (GTO) and the Legacy programs. Deep IRAC observations are also planned for all programs but are not discussed in this paper. The characteristics of all the following surveys are summarized in Table 2.

The MIPS GTO program for cosmological surveys[2] is composed of three surveys, named "Shallow," "Deep," and "Ultra Deep," respectively, whose characteristics are listed in Table 2. The MIPS GTO program also includes galaxy cluster observations, aimed at mapping lensed background galaxies. In addition, some IRAC and IRS GTO programs share the same targets or directly contribute to some of them.

Two of the six Legacy programs are focused on cosmological surveys: the *SIRTF* Wide-Area Infrared Extragalactic survey (SWIRE)[3] and the Great Observatories Origins Deep Survey (GOODS).[4] Schematically, for MIPS observations, the SWIRE surveys have the same observational strategy as the GTO Shallow survey but will cover a larger sky area (65 deg^2), and the GOODS surveys are similar to the GTO Ultra Deep survey but will observe a 0.04 deg^2 field at 24 μm with more depth.

[1] All useful materials regarding the *SIRTF* instruments, including the characteristics and the simulated beam profiles, are available at the SSC Web site: http://sirtf.caltech.edu/SSC.

[2] See http://lully.as.arizona.edu.
[3] See http://www.ipac.caltech.edu/SWIRE.
[4] See http://www.stsci.edu/science/goods.

TABLE 2

MIPS COSMOLOGICAL SURVEY KEY FEATURES

Survey	MIPS Observation Mode[a]	Area[b] (deg^2)	24 μm t_{int}[c] (s)	70 μm t_{int}[c] (s)	160 μm t_{int}[c] (s)
Shallow[d]	Scan medium (2 passes)	9	80	80	8
Deep[d]	Scan slow (12 passes)	2.45 (6×0.41)	1200	1200	120
Ultra Deep[d]	Photometry	0.02	14700	12500	...
Cluster[d]	Photometry	0.2 (28×0.007)	3300	400	80
SWIRE[e]	Scan medium (2 passes)	65 (7 fields)	80	80	8
GOODS[e]	Photometry	0.04	36000	...	...
FLS[f]	Scan medium (2 passes)	5	80	80	8
FLS verification[f]	Scan medium (10 passes)	0.25	400	400	40

[a] MIPS observation mode. For the surveys, two modes are used: photometry and scan map. In the case of scan maps, the rate is given, medium (4 s frame^{-1}) or slow (10 s frame^{-1}), as well as the number of passes.
[b] Total surface of the survey. If more than one field, the details of the number of fields and the approximate size are also given.
[c] Integration time in seconds per sky pixel.
[d] GTO program.
[e] Legacy program.
[f] First Look Survey.

Finally, an early survey in the *SIRTF* mission will be conducted with MIPS and IRAC to verify the observational strategies: the First Look Survey (FLS)[5] of the extragalactic component. Given the similarities with other surveys, we do not discuss this survey specifically.

2.3. *Sensitivity*

The noise in the MIPS instrument is the sum of the detector-related noise (e.g., read noise, linearity correction noise, instantaneous flat-field noise), cosmic rays, and photon noise. The noise budget is dominated by photon noise (G. H. Rieke 2002, private communication). For simplicity, we call the total noise "photon noise" (σ_p), even if all the instrumental noise sources are taken into account. Table 1 gives the 1 σ_p noise in scan map mode for a 10 s integration (scan map mode or photometry mode). The upper part of Table 5 gives the 1 σ_p noise for the different integrations planned for the surveys. Note that noise caused by any systematic effect is not taken into account here. It has been shown for ISOCAM, however, that the latter noise source does not degrade the final sensitivity (Miville-Deschênes et al. 2000).

3. CIRRUS CONFUSION NOISE

Previous works (Helou & Beichman 1990; Gautier et al. 1992; Kiss et al. 2001) studied in detail the confusion noise due to Galactic cirrus ($\sigma_{\rm Gc}$) and showed that in most cases it can be simply parameterized as follows:

$$\sigma_{\rm Gc} = 0.3(\lambda_{100})^{2.5}(D_m)^{-2.5}\langle B_\lambda\rangle^{1.5}\ , \qquad (1)$$

where $\sigma_{\rm Gc}$ is in mJy, λ_{100} is the wavelength ratio $\lambda/(100\ \mu{\rm m})$, D_m is the telescope diameter in meters, and $\langle B_\lambda\rangle$ is the brightness in MJy sr^{-1} (Helou & Beichman 1990). Kiss et al. (2001) report that this parameterization underestimates $\sigma_{\rm Gc}$ by a factor of 2. However, their estimate of $\sigma_{\rm Gc}$ includes a contribution from CIB fluctuations that is known to be significant (Lagache & Puget 2000), and so we can use the parameterization when we are only concerned with the Galactic cirrus component

Using Figure 1 of Boulanger (2000) for the spectrum of the diffuse ISM, we extrapolate the mean brightness at 100 μm $\langle B_{100}\rangle$ of 0.5 MJy sr^{-1} (corresponding to an H I column density of 10^{20} cm^{-2}, typical for cosmological surveys) at 24, 70, and 160 μm. We then derive the corresponding cirrus confusion noise $\sigma_{\rm Gc}$ from equation (1). The results are given in Table 3. For most of the cosmological fields, where the cirrus brightness $\langle B_{100}\rangle$ is less than 1 MJy sr^{-1}, the cirrus confusion noise is often negligible or is a minor contribution to the total noise. In this work, we thus only consider the confusion due to extragalactic sources, letting the reader add the cirrus confusion noise appropriate to his or her own purposes.

[5] See http://sirtf.caltech.edu/SSC/fls/extragal.

TABLE 3
CIRRUS CONFUSION NOISE

Parameter	24 μm	70 μm	160 μm
$\langle B_\lambda\rangle$[a] (MJy sr^{-1}).....	0.03	0.12	1.5
$\sigma_{\rm Gc}$[b]	0.06 μJy	7.6 μJy	2.7 mJy

[a] Cirrus brightness for MIPS bands. This cirrus has a brightness $\langle B_{100}\rangle = 0.56$ MJy sr^{-1} at 100 μm, corresponding to $N_{\rm H\,I} = 10^{20}$ cm^{-2}. We use the dust spectrum from Boulanger (2000).

[b] The 1 $\sigma_{\rm Gc}$ cirrus confusion noise derived from eq. (1) (Helou & Beichman 1990).

4. MODEL OF INFRARED GALAXY EVOLUTION

In addition to the photon noise and cirrus confusion noise, the noise due to extragalactic sources is certainly the dominant noise for cosmological surveys. The Lagache et al. (2003) model is used to describe this component.

This model fits, besides the CIB intensity, source counts, the redshift distribution and colors, and the additional observational constraint of the CIB fluctuations. It describes only the dust emission part of the galaxies in the 4 μm to 1.5 mm wavelength range. It is a phenomenological model based on two galaxy populations: the IR emission of normal spiral galaxies where optical output dominates and a starburst population. Each population is characterized by a SED family and an evolving luminosity function, described by a small number of parameters. The predictions of this model thus cover well the observed wavelength range from 8 μm to 3 mm. It does not include source clustering. The confusion is computed for the Poisson contribution, and the clustering might slightly change the confusion limits; this will be investigated in forthcoming papers (J. Blaizot et al. 2003, in preparation; M. Sorel et al. 2003, in preparation). The model outputs as well as some programs are publicly available on our Web sites.[6]

5. SIMULATING THE MULTIWAVELENGTH INFRARED SKY

One of the applications of the model of Lagache et al. (2003) for planning future observations is the creation of simulated maps of the infrared and submillimeter sky. The main purposes of the simulations are (1) to test the calibration and map-making algorithms, (2) to test and validate the source extraction and photometry procedures and check the completeness, and (3) to test other algorithms, such as HIRES or band-merging procedures, to improve source detections in the FIR range. Results of these simulations will be the subject of a forthcoming paper.

The maps,[7] available for public use upon request, are sampled with 2″ pixels and have sizes ranging from 1024^2 to 4096^2 (0.32–5 deg^2). The simulated maps contain three components: an extragalactic component (IR galaxies), a Galactic foreground component (cirrus), and a zodiacal light component. The following is a brief description of each component.

The Lagache et al. (2003) model evolving luminosity functions are used to create the extragalactic component in simulated maps over a wide range of wavelengths relevant to current and future studies (mainly for *ISO*, *SIRTF*, *ASTRO-F*, *Planck*, *Herschel*, SCUBA, MAMBO, and ALMA). For computational efficiency, we add in the maps sources only in the redshift range 0–5.

[6] See http://www.ias.fr/PPERSO/glagache/act/gal_model.html and http://lully.as.arizona.edu/Model.

[7] Images of the maps are available on our Web site, http://lully.as.arizona.edu/GTODeep/Simulations.

The Galactic foreground component, the cirrus, is built as follows: the spatial structure is taken from an actual 100 μm cirrus in the *IRAS* recalibrated maps of Schlegel, Finkbeiner, & Davis (1998), and the scale extrapolation to smaller scales uses the properties of the cirrus power spectrum from Gautier et al. (1992). We then use the cirrus spectrum of Boulanger (2000) to compute this component at other wavelengths.

The zodiacal light component is a constant value in our maps, taken from Table 4 of Kelsall et al. (1998) for high ecliptic and Galactic latitude fields.

6. DERIVING THE CONFUSION NOISE DUE TO EXTRAGALACTIC SOURCES

Numerous authors (Condon 1974; Hacking, Houck, & Condon 1987; Hacking & Soifer 1991; Franceschini et al. 1989, 1991; Vaisanen, Tollestrup, & Fazio 2001) have described the effect of the fluctuations due to the presence of point sources in a beam. For technological reasons limiting the telescope diameter compared to the wavelength, these fluctuations play an important (if not dominant) role in the measurements noise budget in the MIR, FIR, submillimeter, and centimeter range for extragalactic surveys.

Throughout the rest of the paper, we use the term "confusion limit" for the confusion limit due to extragalactic sources. There are two different criteria to derive the confusion noise. The widely-used "photometric criterion" (§ 6.3) is derived from the fluctuations of the signal due to the sources below the detection threshold $S_{\rm lim}$ in the beam; it was well adapted for the first generation of space IR telescopes (*IRAS*, *COBE*, *ISO*). The "source density criterion" (§ 6.4) is derived from a completeness criterion and evaluates the density of the sources detected above the detection threshold $S_{\rm lim}$, such that only a small fraction of sources are missed because they cannot be separated from their nearest neighbor.

We show that with *SIRTF* (or other planned telescopes), we need in general (regardless of the model used) to compare the confusion noise given by the two criteria, in order not to artificially underestimate the derived confusion noise. We give our estimates for the confusion in the frame of the Lagache et al. (2003) model.

6.1. *Confusion Noise: General Case*

At a given frequency ν (hereafter the subscript ν will be omitted), let $f(\theta, \phi)$ be the two-dimensional beam profile (peak normalized to unity), let S be the source flux density (hereafter flux) in Jy, and let dN/dS be the differential source counts in $\mathrm{Jy}^{-1}\,\mathrm{sr}^{-1}$.

The amplitude of the response x due to a source of flux S at location θ, ϕ within the beam is

$$x = Sf(\theta, \phi) \; . \tag{2}$$

The mean number of responses $R(x)$ with amplitudes between x and $x + dx$ from sources present in the beam element $d\Omega$ at position (θ, ϕ) (where $d\Omega = 2\pi\theta\, d\theta\, d\phi$) is given by

$$R(x)dx = \int_{\Omega} \frac{dN}{dS} dS\, d\Omega \; . \tag{3}$$

The total variance σ_c^2 of a measurement within the beam due to extragalactic sources of fluxes less than $S_{\rm lim}$ is given by

$$\sigma_c^2 = \int_0^{x_{\rm lim}} x^2 R(x) dx \; , \tag{4}$$

where $x_{\rm lim} = S_{\rm lim} f(\theta, \phi)$ is the cutoff response at high flux. This can be rewritten as

$$\sigma_c^2 = \int f^2(\theta, \phi) d\theta\, d\phi \int_0^{S_{\rm lim}} S^2 \frac{dN}{dS} dS \; . \tag{5}$$

We call σ_c the "confusion noise" and $S_{\rm lim}$ the "confusion limit." There are different ways of deriving $S_{\rm lim}$, and they will be investigated in §§ 6.3 and 6.4. Note that using equation (5) to determine the confusion limit is an approximation. A first refinement would be to use the limiting deflection $x_{\rm lim}$ rather than $S_{\rm lim}$, as explained by, e.g., Condon (1974), and then to introduce the effective beam. For MIPS, this changes the confusion level by less than 10%. Nevertheless, this refinement is not enough since it does not take into account other important parameters related to the observational strategy and the analysis scheme, such as the sky sampling, the pixelization (or point-spread function [PSF] sampling), and the source extraction process, that also impact the confusion limit. Only complete realistic simulations would allow for accurately predicting the confusion level; this next step will be addressed in a forthcoming paper using our simulations (§ 5). The method presented here aims at providing a theoretical prediction, which can be considered as a lower limit.

6.2. *Beam Profiles*

Before we obtain measurements of the telescope PSF in flight, we need to use models of the beam profiles for the predictions of the confusion noise. A popular approximation is to use a Gaussian profile with the same FWHM as the expected PSF, although for *SIRTF* an Airy function should be more appropriate. The Gaussian profile is useful for analytical derivations of the confusion level as a function of the beam size (Vaisanen et al. 2001). We want here to address the question of accuracy using the Gaussian approximation, the Airy approximation, or the modeled profile.

We compare the integral of the Gaussian profile (as written in eq. [5]) with the simulated profile obtained by S Tiny Tim (§ 2.1): this leads to a small error in the first integral in equation (5) on the order of 2%–10%, depending on the MIPS wavelength; the difference is larger on the integral of the profile, about 30%. The Gaussian profile is thus a good approximation for computing analytically the confusion noise but not for source extraction simulations.

Using an Airy profile gives better results for the profile integral, with a difference of less than 20%; the difference on the profile integrated according to equation (5) is worse, on the order of 10%–35%. The Airy profile is thus better suited for source extraction simulations than for confusion noise estimates.

The use of the simulated S Tiny Tim profiles (see Table 1) is at present our best approximation of the flight profiles. Indeed, Lagache & Dole (2001) have shown in the case of ISOPHOT that the theoretical profile is in good agreement with the actual profile.

6.3. *The Photometric Criterion for Confusion Noise*

The "photometric criterion" is defined by choosing the signal-to-noise ratio q between the faintest source of flux

TABLE 4
CONFUSION LIMITS WITH DIFFERENT CRITERIA AND FINAL CONFUSION LIMITS

Parameter	24 μm	70 μm	160 μm
$S_{\rm lim}$ and q Using the Photometric Criterion[a]			
$S_{\rm lim}$, $q = 3$	...	0.20 mJy	20 mJy
$S_{\rm lim}$, $q = 4$	7.1 μJy	0.56 mJy	40 mJy
$S_{\rm lim}$, $q = 5$	15.8 μJy	1.12 mJy	56 mJy
$S_{\rm lim}$ and q Using the Source Density Criterion[b]			
$S_{\rm lim}$.....	50 μJy	3.2 mJy	36 mJy
$q_{\rm SDC}$	7.3	6.8	3.8
$S_{\rm lim}$ and q Using the Best Estimator[c]			
$S_{\rm lim}$.....	50 μJy	3.2 mJy	36.0 mJy
q.....	7.3[d]	6.8[d]	3.8[d,e]

[a] $S_{\rm lim}$ using the photometric criterion, for different values of q.
[b] $S_{\rm lim}$ using the source density criterion, and the equivalent values of $q_{\rm SDC}$.
[c] $S_{\rm lim}$ and q of the best confusion estimator. These values are our confusion limits.
[d] Using the source density criterion.
[e] In this case, the photometric and source density criteria agree.

$S_{\rm lim}$ and the rms noise σ_c due to fluctuations from beam to beam (due to sources fainter than $S_{\rm lim}$), as described by

$$q = \frac{S_{\rm lim}}{\sigma_{c\,\rm phot}(S_{\rm lim})} \ ; \tag{6}$$

$S_{\rm lim}$, and thus σ_c, is found by solving equation (6) through an iterative procedure, and q is usually chosen with values between 3 and 5, depending on the objectives followed. Notice that $\sigma_{c\,\rm phot}$ increases with q, as given in the upper part of Table 4. As a guideline, if one assumes a power law for the shape of the differential source counts ($dN/dS \propto S^{\alpha}$, with $|\alpha| < 3$), then $\sigma_{c\,\rm phot}$ varies with q as $\sigma_{c\,\rm phot} \propto q^{-(3+\alpha)/(1+\alpha)}$. This can be used in the Euclidean regime ($|\alpha| = 2.5$). Note that α has the same meaning as $-\gamma$ in Condon (1974).

To illustrate the behavior of the implicit equation (6), Figure 1 gives $S_{\rm lim}/\sigma_{c\,\rm phot}$ as a function of $S_{\rm lim}$ given by equation (5), as well as the constant ratio $q = S_{\rm lim}/\sigma_{c\,\rm phot}$ for $q = 3$ and 5. This plot illustrates that using $q = 3$ at 24 μm does not give a well-defined solution, since the $S_{\rm lim} = 3\ \sigma_{c\,\rm phot}$ line is almost tangent to the curve $\sigma_{c\,\rm phot}(S_{\rm lim})$; in this case, the signal–to–photometric confusion noise ratio is always greater than 3.

6.4. *The Source Density Criterion for Confusion Noise*

A second criterion for the confusion can be defined by setting the minimum completeness of the detection of sources above $S_{\rm lim}$, which is driven by the fraction of sources lost in the detection process because the nearest neighbor with flux above $S_{\rm lim}$ is too close to be separated.[8] For a given source density N (Poisson distribution) corresponding to sources with fluxes above $S_{\rm lim}$, the probability P of having the nearest source of flux $\geq S_{\rm lim}$ located closer than the distance $\theta_{\rm min}$ is

$$P(< \theta_{\rm min}) = 1 - e^{-\pi N \theta_{\rm min}^2} \ . \tag{7}$$

Using $\theta_{\rm FW}$, the FWHM of the beam profile, and k, we parameterize $\theta_{\rm min}$ as

$$\theta_{\rm min} = k\theta_{\rm FW} \ . \tag{8}$$

Fixing a value of the probability P gives a corresponding density of sources $N_{\rm SDC}$ (SDC stands for source density criterion):

$$N_{\rm SDC} = -\frac{\log\,(1 - P(< \theta_{\rm min}))}{\pi k^2 \theta_{\rm FW}^2} \ . \tag{9}$$

At a given wavelength, there is a one-to-one relationship between the source density and the flux, given by the source counts; thus, $S_{\rm SDC}$ is determined with $N_{\rm SDC}$ with our source count model. We identify $S_{\rm SDC}$ as $S_{\rm lim}$ and can then compute the confusion noise using the source density criterion $\sigma_{\rm SDC}$, using equation (5), as a function of P and k.

We define the source density criterion for deriving the confusion noise by choosing values of $P(< \theta_{\rm min})$ and k; the latter can be determined, e.g., by simulations. The term $S_{\rm lim}$ is the limiting flux, such that there is a chosen probability $P(< \theta_{\rm min})$ of having two sources of flux above $S_{\rm lim}$ at a distance of less than $\theta_{\rm min} = k\theta_{\rm FW}$.

We made simulations of source extraction with DAOPHOT and checked that $k = 0.8$ is an achievable value; this is also in agreement with the results from Rieke, Young, & Gautier (1995). We thus use $k = 0.8$. We use $P = 10\%$, meaning that 10% of the sources are too close to another source to be extracted. The corresponding source density is, as explained in Table 1 of Lagache et al. (2003),[9] $(1/16.7)\Omega$.

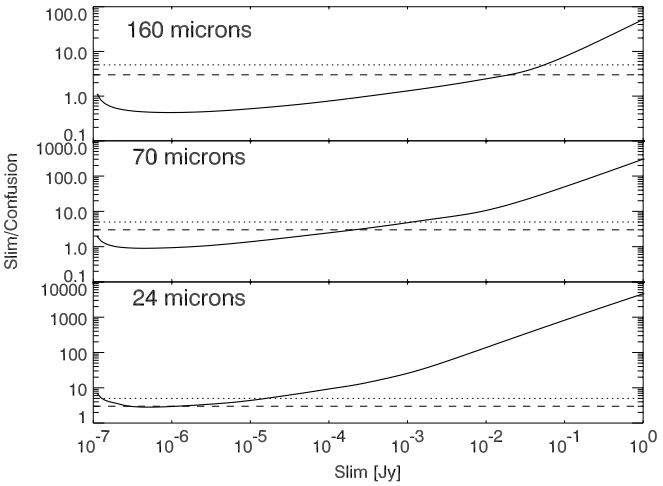

FIG. 1.—Signal–to–confusion noise ratio as a function of $S_{\rm lim}$ at 24, 70, and 160 μm (*solid line*). Also plotted are $S_{\rm lim}/\sigma_c = 3$ (*dashed line*) and $S_{\rm lim}/\sigma_c = 5$ (*dotted line*). At 24 μm, $S_{\rm lim}/\sigma_c$ is always greater than 3; using the photometric criterion for deriving the confusion noise thus leads to a severe underestimation.

[8] The completeness is also affected by the noise that modifies the shape of the source counts, the so-called Malmquist-Eddington bias. For the sake of simplicity, this bias was not taken into account.

[9] Using the relation, valid for both Airy and Gaussian profiles, linking $\theta_{\rm FW}$, the FWHM of the beam profile, and Ω, the integral of the beam profile, $\Omega \simeq 1.14\theta_{\rm FW}^2$ (Lagache et al. 2003).

The middle part of Table 4 gives $S_{\lim \mathrm{SDC}}$, using the source density criterion, and the corresponding equivalent q_{SDC}, which is the ratio $S_{\lim}/\sigma_{\mathrm{SDC}}$.

One the one hand, the photometric and source density criteria give almost identical results in the simple Euclidean case, if one takes $q = 3$, $k = 1$, and a maximum probability of missing a source too close to another one of 10%. In this classical case, confusion becomes important for a source density corresponding to one source per 30 independent instrumental beams. On the other hand, when the relevant $\log N$–$\log S$ function departs strongly from Euclidean, the two criteria give very different results for these reasonable values of q, k, and P. Furthermore, for specific astrophysical problems, one might want to choose significantly different values of these parameters. In that case, the two criteria might not be equivalent. For instance, at 70 μm, increasing P to 20%, 45%, and 60% (instead of the 10% that we are using) gives a confusion limit identical to $q = 5$, 4, and 3, respectively, even if in the last case 60% of the sources are missed.

7. CONFUSION LIMITS FOR MIPS AND COMPARISON WITH OTHER WORKS

7.1. *Confusion Limits for MIPS*

Comparing the photometric (§ 6.3) and the source density (§ 6.4) criteria for the confusion, we conclude that for MIPS, the source density criterion is always met before (i.e., at higher flux) the photometric criterion using $q \simeq 4$. At 160 μm, the two criteria become identical. Lagache et al. (2003) show that for all the IR/submillimeter space telescopes of the coming decade, the break point between the two criteria is around 200 μm.

SIRTF, with its high sensitivity and its well-sampled PSFs, will probe a regime in the source counts where the classical photometric criterion is no longer valid. The main reasons are (1) the steep shape of the source counts and (2) the fact that a significant part of the CIB will be resolved into sources (§ 9.4). This leads to a high source density at faint detectable flux levels, which actually limits the ability to detect fainter sources. In this case, the limiting factor is not the fluctuations of the sources below the detection limit (photometric criterion) but the high source density above the detection limit (source density criterion). For *SIRTF*, we thus use the source density criterion for deriving the confusion noise and limit.

For the previous generations of infrared telescopes (*IRAS*, *ISO*), it is interesting to compare the two criteria, and usually they converge to the same answer—a direct consequence of undersampling a large PSF, which does not allow for probing deeper the source counts. In this case, the photometric criterion is applicable and has been widely used. The confusion noise and the confusion limit for MIPS are given in the lower part of Table 4.

Figure 2 represents the integral source counts at 24, 70, and 160 μm. At these wavelengths, the confusion limits given in Table 4 correspond to source densities of 6.9×10^7, 7.8×10^6, and 1.9×10^6 sr^{-1} at 24, 70, and 160 μm, respectively. This corresponds to 11.5, 12.8, and 12.0 beams source^{-1} at 24, 70, and 160 μm, respectively. The derived values are slightly lower than the "generic" case discussed in § 6.4 of 16.7 sources beam^{-1}, the difference coming from the use of a simulated beam profile rather than a Gaussian profile.

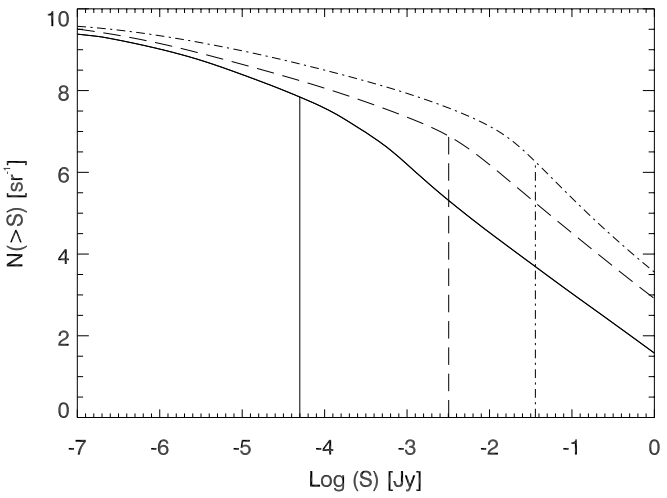

FIG. 2.—Integral source counts from our model at 24 μm (*solid line*), 70 μm (*dashed line*), and 160 μm (*dot-dashed line*) and confusion limits $S_{\lim}$ from Table 4.

7.2. *ISO at 170 μm*

The data of the 4 deg^2 FIRBACK survey (Dole et al. 2001) performed with *ISO* at 170 μm allowed for directly measuring the sky confusion level. This provides a rare opportunity to test the model.

The confusion level was measured at 170 μm at 1 $\sigma_c = 45$ mJy, and the 4 σ_c limit (180 mJy) corresponds to 52 beams source^{-1} (Dole et al. 2001).

Using our model with the actual PSF (Lagache & Dole 2001) and the photometric criterion (valid in this case), we obtain 1 $\sigma_c = 40$ mJy, and for $q = 4$, $S_{\lim} = 158$ mJy; this flux limit corresponds to 40 beams source^{-1}.

The good agreement comforts the quality of the model for estimating the confusion level from modeled source counts.

7.3. *Comparison with Other Determinations*

Xu et al. (2001) computed the confusion limit $S_{\lim}$ with the photometric criterion using $q = 3$ for MIPS and got 33 μJy, 3.9 mJy, and 57 mJy at 24, 70, and 160 μm, respectively. This corresponds respectively to 8, 17, and 31 beams source^{-1}. Our estimates are thus compatible at 70 μm but slightly different at 24 and 160 μm. Their use of the photometric criterion at 24 μm significantly underestimates the confusion level. At 160, their redshift distribution seems to overestimate (at the FIRBACK flux limits) the population peaking at $z \sim 1$ (Patris et al. 2003), which may suggest a difference in the dN/dS distribution, which directly affects the predicted confusion levels.

Franceschini et al. (2003), based on the model of Franceschini et al. (2001), give preliminary 5 σ_c confusion limits for MIPS at 24, 70, and 160 μm as 85 μJy, 3.7 mJy, and 36 mJy, respectively. This corresponds respectively to 19, 15, and 12 beams source^{-1}. The values for the far infrared are in good agreement with our predictions. However, a more refined comparison needs to be done when details of their computation are published, especially in the MIR.

Other models exist (Roche & Eales 1999; Tan et al. 1999; Devriendt & Guiderdoni 2000; Wang & Biermann 2000; Chary & Elbaz 2001; Pearson 2001; Rowan-Robinson 2001b; Takeuchi et al. 2001; Wang 2002) but do not specifi-

cally address the point of predicting the confusion limits for *SIRTF*. Malkan & Stecker (2001) and Rowan-Robinson (2001a) make predictions. The former use, as a photometric criterion, 1 source beam^{-1}. The latter uses 1 source per 40 beams, leading to $S_{\rm lim}$ values of 135 μJy, 4.7 mJy, and 59 mJy at 24, 70, and 160 μm, respectively.

7.4. *The 8 μm Case*

Our model reaches its limit around 8 μm because our SEDs are not designed for wavelengths shorter than 4 μm. However, it fits all observables at wavelengths longer than 7 μm. We can thus predict the confusion level. As for 24 μm, the confusion level will be low and will not limit the extragalactic surveys.

At 8 μm, the photometric criterion does not provide a meaningful confusion limit because the $S_{\rm lim}/\sigma_c$ ratio is always greater than 10. We obtain, using the source density criterion, $S_{\rm lim} = 0.45$ μJy and $\sigma_c = 0.05$ μJy, leading to $q = 9.72$.

The values from Vaisanen et al. (2001) are $S_{\rm lim} = 3$–4 μJy, $\sigma_c = 0.40$–0.51 μJy, and $q = 10.0$. Our estimation of the confusion level for this IRAC band is lower by a factor of $\sim$7. This discrepancy comes in fact from the source counts themselves: we underpredict the source density by a factor of 7–8 in the range of 0.1–1 μJy, even if both models reproduce the *ISO* counts. This is expected from a model that accounts properly for the dust emission but does not model the stellar emission of high-redshift galaxies. When using the counts from Vaisanen et al. (2001), we agree with their published values. Vaisanen et al. (2001), in their § 5.3, discuss the sensitivity of the predicted confusion levels to the shape of the source counts and the constraints of the modeled source counts by the data. Their conclusion is that, although the 7 μm ISOCAM source counts above 50 μJy agree within uncertainties, the models below 1 μJy are not much constrained. As a result, the predictions for the confusion level down to the IRAC sensitivity can be as different as a factor of 10. We confirm this analysis.

8. SENSITIVITY IN THE MIPS FINAL MAPS

In this section we compute the sensitivity of the MIPS surveys as a function of the integration time. The total noise $\sigma_{\rm tot}$ is (Lagache et al. 2003)

$$\sigma_{\rm tot} = \sqrt{\sigma_p^2 + \sigma_c^2 + \sigma_{\rm add}^2}\,, \qquad (10)$$

where σ_p is the photon noise (§ 2.3), σ_c is the confusion noise (§ 7 and Table 4), and $\sigma_{\rm add}$ is the additional confusion noise. This additional confusion noise is only present when the photon noise exceeds the confusion noise: in this case, $\sigma_{\rm add}$ accounts for the confusion due to bright sources above the confusion limit but below the photon noise. When $5\,\sigma_p > S_{\rm lim}$, $\sigma_{\rm add}$ is computed as

$$\sigma_{\rm add}^2 = \int f^2(\theta,\phi)d\theta\,d\phi \int_{S_{\rm lim}}^{5\,\sigma_p} S^2 \frac{dN}{dS} dS\,. \qquad (11)$$

Figure 3 shows $\sigma_{\rm tot}$ and the relative contributions of σ_p, σ_c, and $\sigma_{\rm add}$ as a function of the integration time. It appears that the 160 μm data are confusion limited even with short integrations. At 70 μm, the confusion should dominate the noise for exposures longer than 100 s, and $\sigma_{\rm add}$ is a small component in the first 50 s and negligible thereafter. At

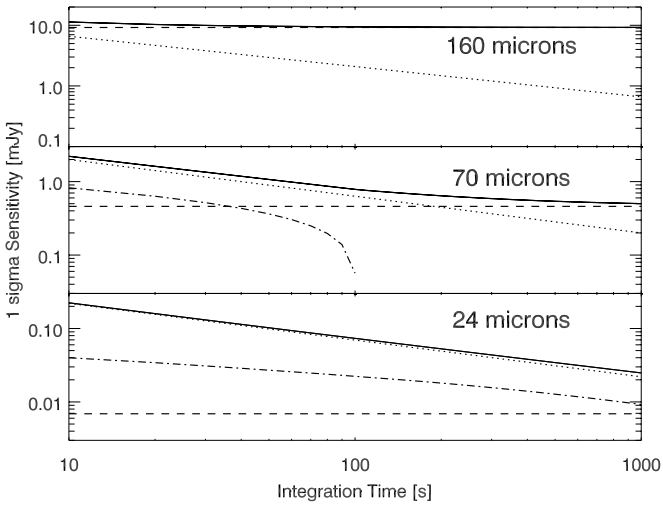

FIG. 3.—The 1 σ sensitivity of the scan maps as a function of integration time at 24, 70, and 160 μm. *Solid line*: Total 1 σ sensitivity. *Dashed line*: Confusion level σ_c. *Dotted line*: Photon noise. *Dot-dashed line*: Additional confusion noise.

24 μm we do not expect the data to be confusion limited, and $\sigma_{\rm add}$ is between 5 and 3 times smaller than the photon noise.

The middle part of Table 5 gives the 1 $\sigma_{\rm tot}$ sensitivity for the surveys and includes the confusion and the instrumental and additional confusion noise components. Note that these 1 $\sigma_{\rm tot}$ values are given as a guideline, knowing that taking 5 $\sigma_{\rm tot}$ for the survey sensitivities is an approximation, since $S_{\rm lim}$ does not equal 5 σ_c in the general case, as discussed in § 7.1.

The bottom part of Table 5 gives the fluxes that will limit the surveys. They are computed by using the approximation given by the quadratic sum $(5\,\sigma_p^2 + S_{\rm lim}^2)^{1/2}$, which provides a smooth transition between the regime dominated by photon/detector noise (24 μm) and the regime dominated by confusion noise (160 μm). These values are taken to be the baseline for further discussions. The final sensitivity for the 65 deg^2 SWIRE Legacy survey will be the same as that for the GTO Shallow survey. The GTO Deep survey will be almost 4 times more sensitive (photon noise) than the Shallow survey, on about 2.5 deg^2; in the FIR, the confusion will nevertheless limit the final sensitivity. For the GOODS Legacy program, with 10 hr of integration per sky pixel at 24 μm on 0.04 deg^2, we expect a final sensitivity of 54 μJy at 24 μm.

It is beyond the scope of this paper to investigate the properties of the galaxy cluster targets of the *SIRTF* GTO program and to make predictions, but in these fields, the confusion limits will significantly be reduced due to the gravitational lensing by a foreground rich cluster, which increases both the brightness and mean separation of the background galaxies. This effect has already been exploited successfully in the MIR (e.g., *ISO*; Altieri et al. 1999) and in the submillimeter (e.g., SCUBA Lens Survey; Smail et al. 2002). The *SIRTF* GTO program will apply the same strategy in the MIR and FIR. The lensed area of the proposed GTO program is expected to cover 90 arcmin^2 (E. Egami 2002, private communication).

Other effects, not included in this analysis, might slightly degrade the final sensitivity of the maps, especially on

TABLE 5

SENSITIVITIES OF THE PLANNED COSMOLOGICAL SURVEYS: 1 σ_p (PHOTON NOISE ONLY), 1 σ_{TOT}, AND FINAL SENSITIVITY

Survey	24 μm	70 μm	160 μm
1 σ_p Sensitivities (Does Not Include Sky Confusion)[a]			
Shallow	78	0.71	6.6
Deep	20	0.18	1.9
Ultra Deep	6	0.06	...
Cluster	12	0.32	2.3
SWIRE	78	0.71	6.6
GOODS	4	...	...
1 σ_{tot} Sensitivities of the Surveys[b]			
Shallow	82	0.87	11.3
Deep	23	0.49	9.4
Ultra Deep	9	0.46	...
Cluster	15	0.55	9.5
SWIRE	82	0.87	11.3
GOODS	8	...	...
Final Sensitivities of the Surveys[c]			
Shallow	392	4.7	48
Deep	112	3.2	36
Ultra Deep	59	3.1	...
Cluster[d]	79	3.5	37
SWIRE	392	4.7	48
GOODS	54	...	...

NOTE.—The values given at 24 μm are in μJy; the values given at 70 and 160 μm are in mJy.

[a] The 1 σ_p sensitivities (they include only photon noise).

[b] The 1 σ_{tot} sensitivities, given as a *guideline*; they includes the confusion, the photon (instrumental), and the additional confusion noise components. Notice that it is *incorrect* to take 5 σ_{tot} as a confusion level for the surveys (see text).

[c] The final sensitivities (see text) of the planned cosmological surveys. They include in a proper manner the confusion noise and photon noise.

[d] The given sensitivities do not take into account here the properties of background lensed galaxies.

TABLE 6

THE NUMBER OF EXPECTED SOURCES IN THE MIPS SURVEYS AND THE FRACTION OF THE CIB THAT WILL BE RESOLVED INTO SOURCES (ASSUMING THAT ALL SOURCES ARE UNRESOLVED)

Survey	24 μm	70 μm	160 μm
Number of Expected Sources			
Shallow	2.0×10^4	1.3×10^4	2.8×10^3
Deep	2.5×10^4	5.8×10^3	1.4×10^3
Ultra Deep	3.7×10^2	49	...
SWIRE	1.5×10^5	1.0×10^5	2.2×10^4
GOODS	8.4×10^2	...	...
Fraction of Resolved CIB (%)			
Shallow	35	46	18
Deep	58	54	23
Ultra Deep	68	54	...
SWIRE	35	46	18
GOODS	69	...	...

NOTE.—The characteristics of the surveys are given in Table 2.

Ge:Ga detectors at 70 and 160 μm; these effects, well characterized on the ground, can probably be corrected with an accuracy of a few percent using data redundancy and a carefully designed pipeline (K. Gordon et al. 2003, in preparation). The effects are stimulator flash latents (the amplitude is less than 3%, and the exponential decay time constant is in the range 5–20 s), transients, responsivity changes (tracked with the stimulator flashes every 2 minutes), and cosmic-ray hit related noise. The final sensitivity will be measured in the first weeks of operation, during the in-orbit checkout and science verification phases.

9. RESOLVED SOURCES: REDSHIFT DISTRIBUTIONS, LUMINOSITY FUNCTION, AND RESOLUTION OF THE COSMIC INFRARED BACKGROUND

9.1. *Source Density and Redshift Distributions*

Many resolved sources are anticipated in the MIPS surveys: for instance, we expect at 160 μm a number of sources more than an order of magnitude higher than those detected by *ISO*, due to both a fainter detection limit and a larger sky coverage. Table 6 gives the number of sources for the GTO and Legacy surveys.

The redshift distributions of the surveys are plotted in Figure 4 for 24 μm, Figure 5 for 70 μm, and Figure 6 for 160 μm. At 24 μm, the deepest fields will allow us to probe the dust emission of sources up to redshift of 2.7. At higher redshifts, the 7.7 μm polycyclic aromatic hydrocarbon (PAH) feature causes a fall in the *K*-correction and thus a decrease in the observed flux close to the sensitivity limit. This is similar to the drop observed with ISOCAM at 15 μm for sources lying at redshift 1.4. (This does not exclude detecting the stellar emission at larger redshifts; this is outside the scope of this paper.)

At 70 μm, the redshift distribution peaks at 0.7, with a tail extending up to redshift 2.5. At 160 μm, the redshift distribution is similar to that at 70 μm. In the FIR, MIPS surveys

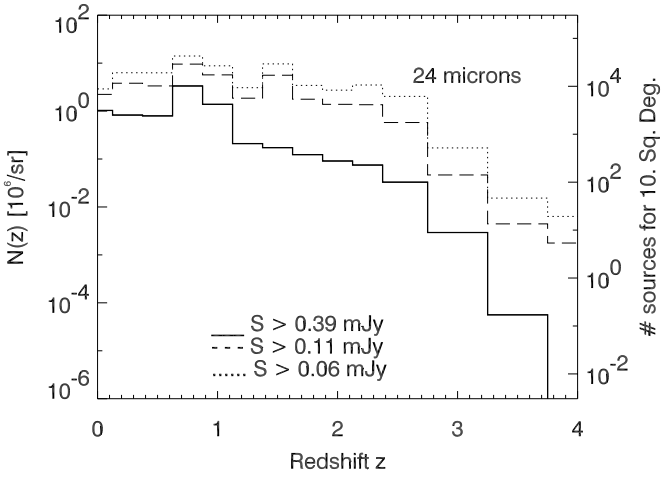

FIG. 4.—Redshift distribution at 24 μm with MIPS. *Solid line*: Shallow survey. *Dashed line*: Deep survey. *Dotted line*: Ultra Deep survey. The flux limits are listed in Table 5. The left axis gives the source density (the number of sources for the particular bin sizes shown); the right axis gives the number of sources in a 10 deg^2 field.

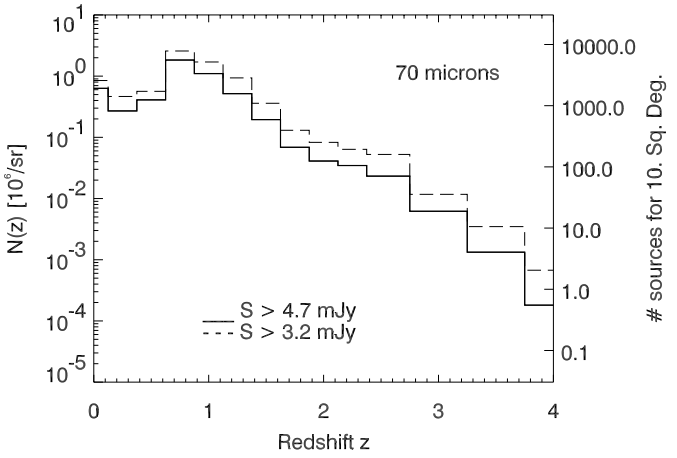

FIG. 5.—Redshift distribution at 70 μm with MIPS. *Solid line*: Shallow survey. *Dashed line*: Deep survey. The flux limits are listed in Table 5. The left axis gives the source density (the number of sources for the particular bin sizes shown); the right axis gives the number of sources in a 10 deg^2 field.

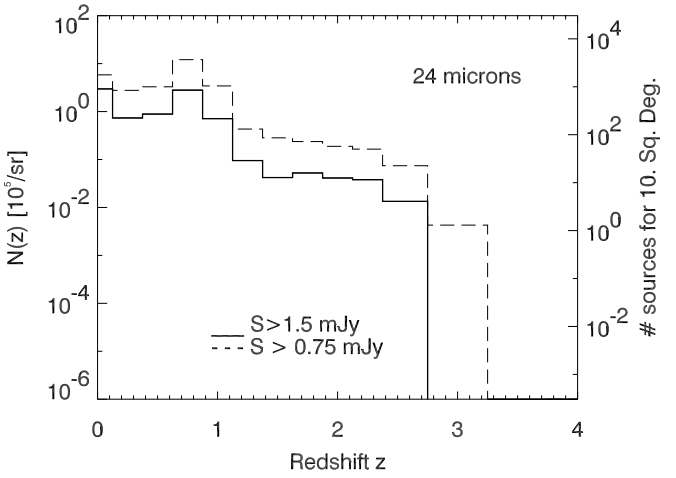

FIG. 7.—Redshift distribution at 24 μm with MIPS for sources brighter than 1.5 and 0.75 mJy, allowing a spectroscopic follow-up with IRS. The left axis gives the source density (the number of sources for the particular bin sizes shown); the right axis gives the number of sources in a 10 deg^2 field. In the proposed 9 deg^2 Shallow survey, we would expect 2100 and 7200 sources to the 1.5 and 0.75 mJy depths, respectively.

will probe extensively the largely unexplored $1 < z < 2.5$ regime.

9.2. *Spectra with IRS*

Spectra of some high-redshift sources will be taken with IRS on board *SIRTF* (as part of the IRS GTO program). With a sensitivity limit of 1.5 mJy at 24 μm and maybe 0.75 mJy (D. Weedman 2002, private communication), a few dozen sources at redshift greater than 2 will be observed. Figure 7 shows the predicted redshift distribution at 24 μm for the Shallow survey of the sources that might be followed up in spectroscopy by IRS.

9.3. *Luminosity Function Evolution*

In addition to the photometric redshifts of a large number of sources and spectroscopic redshift following identifications, building the luminosity function of the sources as a function of redshift will be one of the key results of the *SIRTF* surveys. We show in Figure 8 the source density per logarithmic luminosity bin and per redshift bin expected in the MIPS surveys.

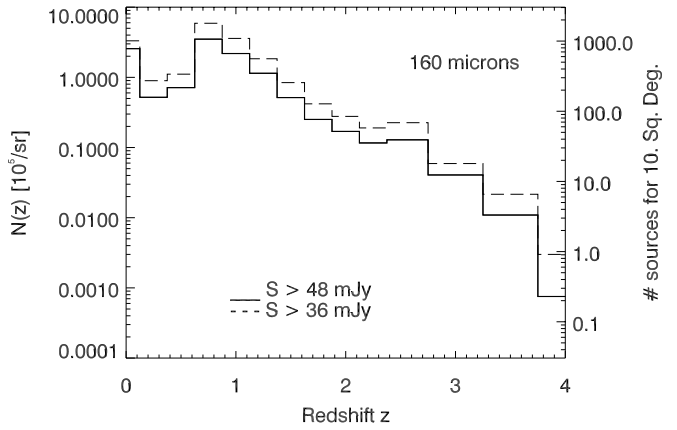

FIG. 6.—Redshift distribution at 160 μm with MIPS. *Solid line*: Shallow survey. *Dashed line*: Deep survey. The flux limits are listed in Table 5. The left axis gives the source density (the number of sources for the particular bin sizes shown); the right axis gives the number of sources in a 10 deg^2 field.

The source density of starburst galaxies is given per logarithmic luminosity bin (of $\Delta \ln L/\ln L = 0.1$) and for redshift bins (of width $\Delta z/z = 0.5$) ranging from $z = 0.01$ to $z = 2.5$. The survey sensitivity cuts the distributions at low luminosities. The size of the surveys limits the ability to derive the luminosity function at high luminosities. The limit of 50 sources per z and L bins is also shown. This limit ensures a statistical accuracy of 14% on the luminosity function for each luminosity and redshift bin; averaging over five bins in luminosity (thus getting $\Delta \ln L/\ln L = 0.5$) allows us to reach an accuracy of 6%.

At 160 μm (Fig. 8, *top*), with a 48 mJy limiting flux and a coverage of 80 deg^2, corresponding to the surface covered by all of the Legacy and GTO extragalactic programs, the MIPS data should allow us to reconstruct the luminosity functions of some ULIRGs ($10^{12}\ L_\odot < L < 3 \times 10^{12}\ L_\odot$) in the $0.5 < z < 0.7$ range, of the $3 \times 10^{12}\ L_\odot < L < 10^{13}\ L_\odot$ galaxies in the $0.5 < z \lesssim 1$ range, and of the HyLIGs (Morel et al. 2001; $L > 3 \times 10^{13}\ L_\odot$) in the $1 \lesssim z \lesssim 2.5$ range.

At 70 μm (Fig. 8, *middle*), with a 4.7 mJy limiting flux and a coverage of 80 deg^2, the sensitivity in the wide and shallow surveys allows us to probe in addition the $3 \times 10^{11}\ L_\odot < L < 10^{12}\ L_\odot$ sources at $z = 0.5$ and the full range $10^{12}\ L_\odot < L < 10^{13}\ L_\odot$ for sources at $0.7 < z < 1$.

At 24 μm, the situation is very similar to that at 70 μm for these shallow surveys (limiting flux of 390 μJy), except for a slightly better sensitivity to galaxies with $L \sim 10^{11}\ L_\odot$ around $z = 0.5$. Concerning deeper and narrower surveys at 24 μm (limiting flux of 112 μJy), such as the GTO Deep survey, the sensitivity to lower luminosity galaxies at higher redshifts is better (Fig. 8, *bottom*). In the redshift range 0.5–2.5, the gain in sensitivity compared to 70 μm allows us to probe galaxies with luminosities lower by a factor of $\sim$5.

9.4. *Resolving the CIB*

To compute the fraction of the CIB that will be resolved into sources, one has to consider the apparent size of the

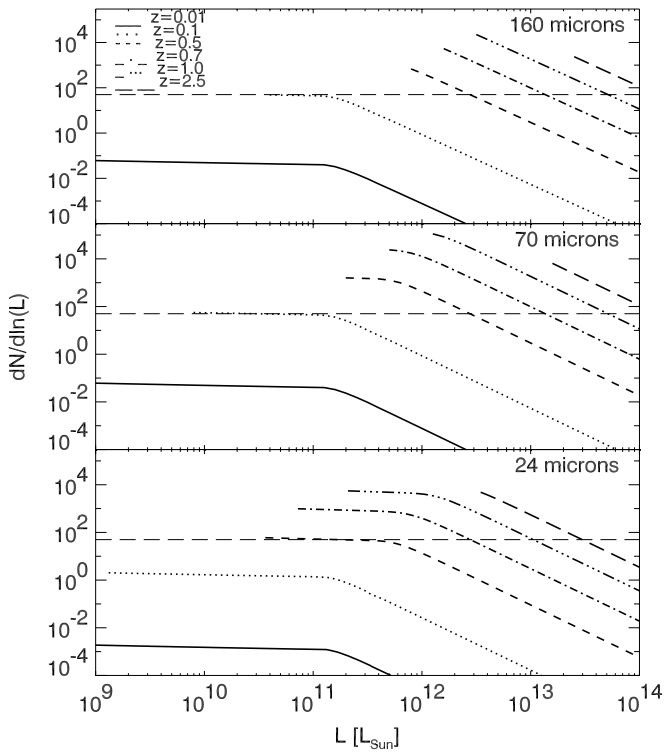

FIG. 8.—Number of starburst galaxies per logarithmic luminosity bin ($\Delta \ln L/\ln L = 0.1$) that can be detected at different redshifts (with $\Delta z/z = 0.5$). *Top*: 160 μm survey of 80 deg^2 (surface covered by SWIRE and GTO) limited by the confusion at 48 mJy. *Middle*: 70 μm survey of 80 deg^2 limited by the confusion at 4.7 mJy. *Bottom*: 24 μm survey of 2.46 deg^2 down to 112 μJy (GTO Deep survey). The horizontal dashed line shows the 50 sources needed in a $\Delta z/z = 0.5$ bin and a $\Delta \ln L/\ln L = 0.1$ bin for reconstructing the luminosity function. From bottom left to top right, the redshift bins are centered at $z = 0.01$, 0.1, 0.5, 0.7, 1.0, and 2.5.

galaxies. Rowan-Robinson & Fabian (1974) give the formalism to deal with resolved and extended sources. To simplify the problem, one might check if all the sources are point sources. For MIPS, the underlying assumption about the physical size of the objects is that it is smaller than 40 kpc, corresponding to less than the FWHM at 24 μm at $z > 1$. Indeed, most of the galaxies observed in the Hubble Deep Field–North with NICMOS exhibit structures smaller than 25 kpc ($\simeq 3''$) in the redshift range $z = 1$–2 (C. Papovich, M. Dickinson, M. Giavalisco, C. Conselice, & H. Ferguson 2003, in preparation). The objects are thus smaller than the MIPS beam sizes and will not be resolved. This might not be the case for IRAC. The closer resolved objects give a negligible contribution to the background anyway.

The fraction of the CIB resolved into discrete sources is given in Table 6. MIPS will resolve at most 69%, 54%, and 24% of the CIB at 24, 70, and 160 μm, respectively. This is an improvement by a factor of at least 3 of the CIB resolution in the FIR over previous surveys (e.g., at 170 μm; Dole et al. 2001). At 24 μm, most of the CIB will be resolved, as ISOCAM did at 15 μm (Elbaz et al. 2002), but with a much wider and deeper redshift coverage.

9.5. *Conclusion: Multiwavelength Infrared Surveys*

In the FIR range, the most promising surveys appear to be the large and shallow ones, because (1) the large number of detected sources is a key to having a statistically significant sample, and (2) the confusion level and the sensitivity are enough to probe sources in the redshift range from 0.7 to 2.5. With significant resolutions of the CIB at 70 and 160 μm (46% and 18%, respectively), the surveys will tremendously improve our knowledge of the sources that *ISO* could not detect. In the MIR range, where the confusion is negligible, the need for deeper surveys is striking. The Deep and Ultra Deep surveys will resolve most of the CIB at 24 μm, allowing us to study not only populations from $z = 0$ to $z = 1.4$ (like *ISO* did) but also the populations that lie at redshifts between 1.5 and 2.7 with unprecedented accuracy (Papovich & Bell 2002). All these multiwavelength surveys (GTO and Legacy programs) will thus probe for the first time a population of infrared galaxies at higher redshifts, allowing us to characterize the evolution, derive the luminosity function evolution, and constrain the nature of the sources, as well as to derive the unbiased global star formation rate up to $z \sim 2.5$.

10. UNRESOLVED SOURCES: FLUCTUATIONS OF THE COSMIC INFRARED BACKGROUND

10.1. *Fluctuation Level and Redshift Distributions*

Sources below the detection limit of a survey create fluctuations. If the detection limit does not allow resolving of the sources dominating the CIB intensity, characterizing these fluctuations gives very interesting information on the spatial correlations of these unresolved sources of cosmological significance. The FIR range is "favored" for measuring the fluctuations, because data are available with very high signal–to–detector noise ratios but limited by the confusion; on the other hand, the confusion limits the possibility of detecting faint resolved sources and leaves the information about faint sources hidden in the fluctuations. The study of the CIB fluctuations is a rapidly evolving field. After the pioneering work of Herbstmeier et al. (1998) with ISOPHOT, Lagache & Puget (2000) discovered them at 170 μm in the FIRBACK data, followed by other works at 170 and 90 μm (Matsuhara et al. 2000; Kiss et al. 2001; Puget & Lagache 2000) and at 60 and 100 μm in the *IRAS* data (Miville-Deschênes, Lagache, & Puget 2002).

Our model reproduces the measured fluctuation levels within a factor of 1.5 between 60 and 170 μm (Lagache et al. 2003). For MIPS, we predict that the level of the fluctuations will be 6930 Jy^2 sr^{-1} at 160 μm for $S_{160} < 48$ mJy and 113 Jy^2 sr^{-1} at 70 μm for $S_{70} < 4.7$ mJy.

Our model gives access to the redshift distribution of the sources dominating the observable fluctuations of the unresolved background. At 170 μm (Fig. 12 of Lagache et al. 2003), the redshift distribution of the contributions to the fluctuations peaks at $z = 0.8$, with a tail up to $z \sim 2.5$, and there is a nonnegligible contribution from local sources. The peak of this distribution is similar to the one of the 15 μm ISOCAM redshift distribution of resolved sources (Elbaz et al. 2002), which are understood to represent a significant fraction of the CIB. These sources observed at two different wavelengths should tell us the same story about galaxy evolution. The key point of studying the fluctuations in the FIR is the availability of large-area surveys to exhibit the source-clustering properties; this is not yet possible with MIR data that need to be taken with deeper (and thus with less area coverage) exposures to probe the same sources. Furthermore, a nonnegligible contribution comes from higher

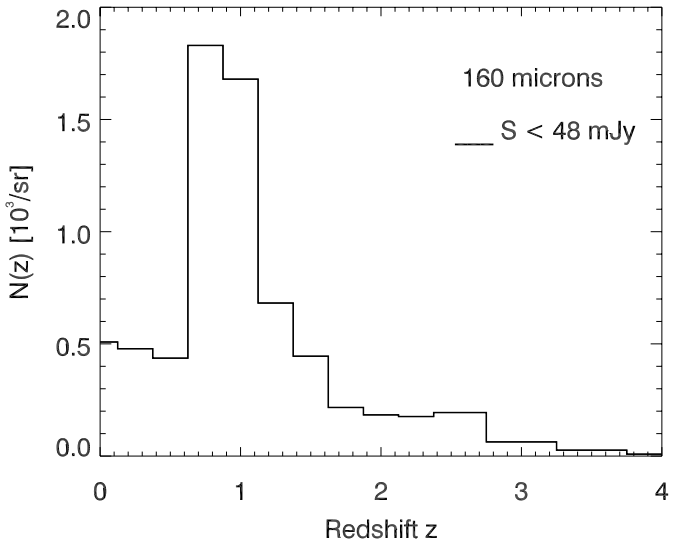

FIG. 9.—Redshift distribution of the sources below 48 mJy creating the fluctuations, at 160 μm with MIPS. The number of sources is shown for the particular bin sizes.

redshifts. Extracting this component will be a challenge requiring the use of all *SIRTF* bands.

At 160 μm (Fig. 9), for the same reasons, the distribution of the sources dominating the fluctuations peaks at $z = 0.8$, with a broad peak from $z = 0.7$ to $z = 1.1$. The tail extends up to $z \sim 2.5$, and the contribution of local sources is less prominent than at 170 μm with the ISOPHOT sensitivity. At 70 μm (Fig. 10), the distribution is similar to that at 160 μm, but with a factor of 3 less source density since the background is half-resolved into sources.

10.2. *Power Spectrum Analysis: Fluctuations and Source Clustering*

The Poisson component of the fluctuations of the CIB has been detected in the FIR by Lagache & Puget (2000) in the FIRBACK data, at spatial frequencies (or wavenumbers) of 0.25 arcmin$^{-1} < k < 0.6$ arcmin^{-1}. A preliminary study on larger fields seems to show that the source clustering is present in the data as well (Puget & Lagache 2000), and this is currently under investigation (M. Sorel et al. 2003, in preparation). However, to accurately constrain the source clustering, larger fields than FIRBACK are needed. Since *SIRTF* will cover larger sky areas, the clustering should be detected and measured in a power spectrum analysis similar to the one done by Lagache & Puget (2000) and Miville-Deschênes et al. (2002).

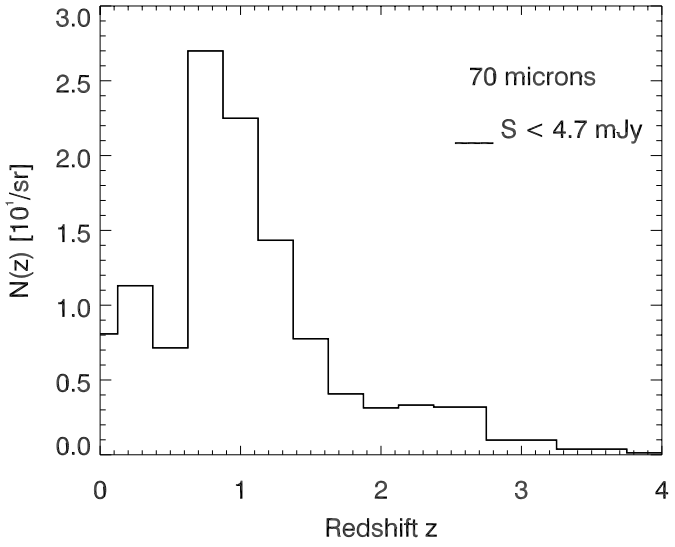

FIG. 10.—Redshift distribution of the sources below 4.7 mJy creating the fluctuations, at 70 μm with MIPS. The number of sources is shown for the particular bin sizes.

We make an estimation of the spatial frequency range where the CIB fluctuations will be detected in the large and shallow surveys at 160 μm, using our model. It does not include source clustering; we simply assume a Poisson distribution of the sources. The detectability of the source clustering is addressed below.

We use the same technique as Lagache & Puget (2000) and Puget & Lagache (2000); following their formalism, the power spectrum measured on the map ($P_{\rm map}$) in the space of the detector can be written as follows:

$$P_{\rm map} = P_{\rm noise} + (P_{\rm cirrus} + P_{\rm sources}) W_k \ , \qquad (12)$$

where $P_{\rm noise}$, $P_{\rm cirrus}$, and $P_{\rm sources}$ are the power spectra of the photon/detector noise, the foreground cirrus, and the extragalactic sources we are interested in, respectively, and W_k is the power spectrum of the PSF. In this analysis, we want to exhibit $P_{\rm sources}$ and, for convenience, $P_{\rm cirrus}$.

Figure 11 shows a prediction for the various components present at 160 μm in a survey like the GTO Shallow survey or SWIRE. The Poisson component for the fluctuations due to extragalactic sources fainter than 48 mJy ($P_{\rm sources}$) is

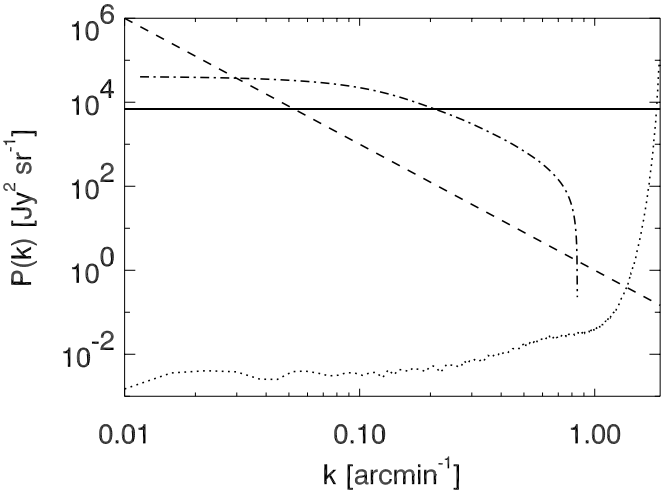

FIG. 11.—Theoretical power spectrum of a 5 deg^2 field at 160 μm, illustrating the spatial frequency range where the CIB fluctuations will be detected (see § 10.2). *Solid line*: Level of CIB Poisson fluctuations created by sources below 48 mJy predicted by our model (6930 Jy^2 sr^{-1}). *Dashed line*: Foreground cirrus, $P_{\rm cirrus}$, with the k^{-3} behavior and normalized at 10^6 Jy^2 sr^{-1} at $k = 0.01$ arcmin^{-1}, representing a column density of $N_{\rm H\,I} = 10^{20}$ cm^{-2}. *Dotted line*: White noise (1 σ of 7 mJy) divided by the PSF, $P_{\rm noise}/W_k$. *Dot-dashed line*: Model source clustering of starburst galaxies of Perrotta et al. (2001) in the case of 170 μm. The wavenumber range of cosmological interest is thus from 0.07 to 1.3 arcmin^{-1}, where the CIB Poisson fluctuations are expected to be detected; assuming the source clustering has the form predicted by Perrotta et al. (2001), it will be detected in the wavenumber range from 0.04 to 0.2 arcmin^{-1}.

shown as the horizontal line, at the value of 6930 $Jy^2\ sr^{-1}$ predicted by the model (see § 10.1); P_{cirrus} is shown as the dashed line and follows a k^{-3} power law (Gautier et al. 1992; Miville-Deschênes et al. 2002). The normalization at $10^6\ Jy^2\ sr^{-1}$ at $k = 10^{-2}$ arcmin^{-1} is typical of the faint cirrus present in the cosmological fields of column density $N_{HI} = 10^{20}\ cm^{-2}$. Finally, P_{noise}/W_k is plotted as a dotted line. The noise is a white noise of 1 σ of 7 mJy, typical for shallow surveys at 160 μm (Table 5).

To have an estimation of the spatial frequency range where the Poisson fluctuations from the extragalactic component will be detected, one has to consider the two limiting components: Galactic cirrus at low spatial frequencies and photon noise plus PSF shape at large spatial frequencies. It appears that the CIB Poisson fluctuations, or the fluctuations created by faint extragalactic sources only, should be well detected in the wavenumber range 0.07 arcmin^{-1} $< k <$ 1.3 arcmin^{-1}.

Taking into account the source clustering, we assume that it is dominated by starburst galaxies with the form predicted by Perrotta et al. (2001).[10] This clustered component is plotted in Figure 11 as a dot-dashed line and has been computed for 170 μm. This component should be detected in the wavenumber range from 0.04 to 0.2 arcmin^{-1}. The cirrus limits the detection at smaller wavenumbers and is the main limitation for the source-clustering detection. The Poissonian component of extragalactic sources limits the detection at larger wavenumbers.

The large shallow surveys in the FIR are thus the most promising for studying the fluctuations and estimating the source clustering (0.04 arcmin^{-1} $< k <$ 0.2 arcmin^{-1}).

11. CONCLUSION

In this work, we review the sources of noise expected in the cosmological surveys to be conducted by MIPS: photon/detector noise, cirrus noise, and confusion noise due to extragalactic sources. Using the Lagache et al. (2003) model, as well as the latest knowledge of the MIPS preflight characteristics (in particular, the photon/detector noise properties and the beam shapes), we predict the confusion levels, after a detailed discussion on the criteria. In particular, we show that in general the criteria depend on the shape of the source counts and the solid angle of the beam (directly related to the telescope and detector pixel size). *SIRTF* is about to probe a new regime in the source counts, where a significant fraction of the CIB is resolved and the counts begin to flatten. We thus discuss the classical rules of determining the confusion level (essentially valid for *IRAS* or *ISO*), and we show that it is wise to compare the photometric and source density criteria for predicting the confusion level. We find S_{lim} to be 50 μJy, 3.2 mJy, and 36 mJy at 24, 70, and 160 μm, respectively, consistent with *ISO* data and other works.

We compute the final sensitivity of the MIPS surveys, the GTO (Guaranteed Time Observer) program and the two Legacy programs (SWIRE and GOODS), predict the number of sources, and give the redshift distributions of the detected sources at 24, 70, and 160 μm. The deepest surveys should detect the dust emission of sources up to $z = 2.7$ at 24 μm (the redshifted 7.7 PAH feature causes a drop of detectability at higher redshifts) and up to $z = 2.5$ at 70 and 160 μm. This corresponds to a resolution of the CIB into discrete sources of 69%, 54%, and 24% at 24, 70, and 160 μm, respectively. We estimate that in the shallow surveys, the sources will be detected in a sufficient number in redshift bins for reconstructing the luminosity function and its evolution with redshift with a 14% (or better) accuracy as follows: most of the $L > 10^{12}\ L_\odot$ sources for $0.5 \lesssim z \lesssim 1$ in the FIR range, most of the $L > 10^{11}\ L_\odot$ sources for $0.5 \lesssim z \lesssim 1$ in the MIR range, and all of the $L \gtrsim 10^{13}\ L_\odot$ sources for $z \simeq 2.5$ in the MIR and FIR range. We also show that at 24 μm, deeper and narrower surveys will considerably increase the sensitivity to lower luminosity galaxies.

We also explore some characteristics of the unresolved sources at long wavelength, among which is the redshift distribution of the contribution to the background fluctuations at 70 and 160 μm. It peaks at $z \sim 0.8$, consistent with our present understanding of the main contribution to the CIB. We estimate the wavenumber range where the large FIR surveys will be able to measure the fluctuations of the Poisson component in a power spectrum analysis as 0.07 arcmin^{-1} $< k <$ 1.3 arcmin^{-1}. With some assumption about the source clustering, we show that it could be detected in the wavenumber range 0.04 arcmin^{-1} $< k <$ 0.2 arcmin^{-1}.

We emphasize the complementary role of large and shallow surveys in the FIR and smaller but deeper surveys in the MIR. The MIR surveys allow us to probe directly faint sources, and the FIR surveys allow us to access the statistical properties of the faint population, mainly through CIB fluctuation analysis. With the various sky area coverages and depths, the MIPS surveys (together with IRAC data helping to estimate the photometric redshifts) will greatly improve our understanding of galaxy evolution by providing data with unprecedented accuracy in the MIR and FIR range.

We thank George and Marcia Rieke for many interesting discussions, as well as Almudena Alonso-Herrero, Eiichi Egami, and Casey Papovich. We also thank Petri Vaisanen for helpful discussions about the 8 μm source counts and for having provided us with his predictions, as well as Francesca Perrotta and Manuela Magliocchetti for having provided us with an electronic version of their model. We also appreciate remarks from Alberto Franceschini and Kevin Xu and discussions with Dario Fadda and Dan Weedman. We thank the referee for the constructive comments and suggestions. H. D. acknowledges the funding from the MIPS project, which is supported by NASA through the Jet Propulsion Laboratory, subcontract P435236, and the Programme National de Cosmologie and the Centre National d'Etudes Spatiales for travel funding.

[10] Other predictions exist in the submillimeter range, but not specifically for 160 μm (Haiman & Knox 2000; Knox et al. 2001). The source clustering is there expected at scales between 0°.1 and 3°.

REFERENCES

Altieri, B., et al. 1999, A&A, 343, L65
Boulanger, F. 2000, in *ISO* Beyond Point Sources: Studies of Extended Infrared Emission, ed. R. J. Laureijs, K. Leech, & M. F. Kessler (ESA SP-455; Noordwijk: ESA), 3
Chary, R., & Elbaz, D. 2001, ApJ, 556, 562
Condon, J. J. 1974, ApJ, 188, 279
Devriendt, J. E. G., & Guiderdoni, B. 2000, A&A, 363, 851
Dole, H., et al. 2000, in *ISO* Surveys of a Dusty Universe, ed. D. Lemke, M. Stickel, & K. Wilke (Lecture Notes in Physics 548; Berlin: Springer), 54
———. 2001, A&A, 372, 364
Elbaz, D., Cesarsky, C. J., Chanial, P., Aussel, H., Franceschini, A., Fadda, D., & Chary, R. R. 2002, A&A, 384, 848
Engelbracht, C. W., Young, E. T., Rieke, G. H., Rivlis, G., Beeman, J. W., & Haller, E. E. 2000, Exp. Astron., 10, 403
Fazio, G. G., et al. 1998, Proc. SPIE, 3354, 1024
Franceschini, A., Aussel, H., Cesarsky, C. J., Elbaz, D., & Fadda, D. 2001, A&A, 378, 1
Franceschini, A., Toffolatti, L., Danese, L., & De Zotti, G. 1989, ApJ, 344, 35
Franceschini, A., Toffolatti, L., Mazzei, P., Danese, L., & De Zotti, G. 1991, A&AS, 89, 285
Franceschini, A., et al. 2003, in The Mass of Galaxies at Low and High Redshift, ed. R. Bender & A. Renzini (New York: Springer), in press
Gautier, T. N. I., Boulanger, F., Perault, M., & Puget, J.-L. 1992, AJ, 103, 1313
Genzel, R., & Cesarsky, C. J. 2000, ARA&A, 38, 761
Hacking, P., Houck, J. R., & Condon, J. J. 1987, ApJ, 316, L15
Hacking, P. B., & Soifer, B. T. 1991, ApJ, 367, L49
Haiman, Z., & Knox, L. 2000, ApJ, 530, 124
Heim, G. B., et al. 1998, Proc. SPIE, 3356, 985
Helou, G., & Beichman, C. A. 1990, in From Ground-based to Space-borne Sub-mm Astronomy (ESA SP-314; Paris: ESA), 117
Herbstmeier, U., et al. 1998, A&A, 332, 739
Houck, J. R., & Van Cleve, J. E. 1995, Proc. SPIE, 2475, 456
Kelsall, T., et al. 1998, ApJ, 508, 44
Kiss, C., Abraham, P., Klaas, U., Juvela, M., & Lemke, D. 2001, A&A, 379, 1161
Knox, L., Cooray, A., Eisenstein, D., & Haiman, Z. 2001, ApJ, 550, 7
Krist, J. 1993, in ASP Conf. Ser. 52, Astronomical Data Analysis Software and Systems II, ed. R. J. Hanisch, R. J. V. Brissenden, & J. Barnes (San Francisco: ASP), 536
Lagache, G., & Dole, H. 2001, A&A, 372, 702
Lagache, G., Dole, H., & Puget, J.-L. 2003, MNRAS, in press
Lagache, G., & Puget, J.-L. 2000, A&A, 355, 17
Malkan, M. A., & Stecker, F. W. 2001, ApJ, 555, 641
Matsuhara, H., et al. 2000, A&A, 361, 407
Miville-Deschênes, M. A., Boulanger, F., Abergel, A., & Bernard, J. P. 2000, A&AS, 146, 519
Miville-Deschênes, M. A., Lagache, G., & Puget, J.-L. 2002, A&A, 393, 749
Morel, T., et al. 2001, MNRAS, 327, 1187
Papovich, C., & Bell, E. F. 2002, ApJ, 579, L1
Patris, J., Dennefeld, M., Lagache, G., & Dole, H. 2003, A&A, submitted
Pearson, C. P. 2001, MNRAS, 325, 1511
Perrotta, F., Magliocchetti, M., Baccigalupi, C., Bartelmann, M., De Zotti, G., Granato, G. L., Silva, L., & Danese, L. 2001, MNRAS, 338, 623
Puget, J.-L., & Lagache, G. 2000, in IAU Symp. 204, The Extragalactic Infrared Background and Its Cosmological Implications, ed. M. Harwit & M. G. Hauser (San Francisco: ASP), 59
Rieke, G. H., Young, E. T., & Gautier, T. N. 1995, Space Sci. Rev., 74, 17
Rieke, G. H., et al. 1984, BAAS, 16, 906
Roche, N., & Eales, S. A. 1999, MNRAS, 307, 111
Rowan-Robinson, M. 2001a, ApJ, 549, 745
———. 2001b, NewA Rev., 45, 631
Rowan-Robinson, M., & Fabian, A. 1974, MNRAS, 167, 419
Schlegel, D. J., Finkbeiner, D. P., & Davis, M. 1998, ApJ, 500, 525
Smail, I., Ivison, R. J., Blain, A. W., & Kneib, J.-P. 2002, MNRAS, 331, 495
Takeuchi, T. T., Ishii, T. T., Hirashita, H., Yoshikawa, K., Matsuhara, H., Kawara, K., & Okuda, H. 2001, PASJ, 53, 37
Tan, J. C., Silk, J., & Balland, C. 1999, ApJ, 522, 579
Vaisanen, P., Tollestrup, E. V., & Fazio, G. G. 2001, MNRAS, 325, 1241
Wang, Y. P. 2002, A&A, 383, 755
Wang, Y. P., & Biermann, P. L. 2000, A&A, 356, 808
Werner, M. W., & Fanson, J. L. 1995, Proc. SPIE, 2475, 418
Xu, C., Lonsdale, C. J., Shupe, D. L., O'Linger, J., & Masci, F. 2001, ApJ, 562, 179
Young, E. T., et al. 1998, Proc. SPIE, 3354, 57